The paper was published in the proceedings of the 20th International Conference on Soil Mechanics and Geotechnical Engineering and was edited by Mizanur Rahman and Mark Jaksa. The conference was held from May 1st to May 5th 2022 in Sydney, Australia.

Proceedings of the 20th International Conference on Soil Mechanics and Geotechnical Engineering– Rahman and Jaksa (Eds)

Side anchored flexible barriers subjected to debris flow impact

Barrière flexibles ancrées au bord soumises à l'impact d'une coulée de débris

Sunil Poudyal, Aastha Bhatta & Charles Wang Wai Ng
Department of Civil and Environmental Engineering, The Hong Kong University of Science and Technology, HKSAR China, spoudyal@connect.ust.hk

Clarence Edwards Choi
Department of Civil Engineering, The University of Hong Kong, HKSAR China

Harris W K Lam & Eric H Y Sze
Geotechnical Engineering Office, Civil Engineering and Development Department, The Government of Hong Kong SAR, Hong Kong SAR

ABSTRACT: Flexible barriers are commonly installed in mountainous slopes to intercept landslides, rockfalls and debris flows. The lack of reliable and systematic studies has limited our understanding of complex debris flow-flexible barrier interaction. As a consequence, a globally accepted flexible barrier design guideline is lacking. In this study, side anchored flexible barrier subjected to channelized debris flow impact is modelled in a state-of-the-art 28 m-long and 2 m-wide flume facility in Hong Kong. The response of a side anchored flexible barrier impacted by a single surge of debris flow is studied. The primary focus of this study is to investigate the role of energy dissipating brake elements in attenuating peak impact force on load bearing cables. Novel energy dissipating brake elements developed in-house at HKUST are used. Impact forces on flexible barriers are measured by tension load cells installed at anchors supporting load bearing cables. Preliminary result shows side anchored flexible barrier with brake elements reduces peak cable loads and increases energy dissipation.

RÉSUMÉ: Les barrières flexibles sont souvent installées dans les territoires de montagne pour arrêter les glissements de terrain, les chutes de pierres et les écoulements de débris. Le manque d'études fiables et systématiques a limité notre compréhension de l'interaction complexe entre la barrière flexible et les coulées de débris. En conséquence, il n'y a aucun cadre normatif pour le projet des barrières flexibles qui est internationalement accepté. Dans cette étude, l'impact de la coulée de débris sur une barrière flexible ancrée au bord est testée dans un canal expérimental, à l'état de l'art, situé en Hong Kong, avec une longueur de 28m et une largeur de 2m. La réponse de la barrière flexible à l'impact d'une seule coulée est étudié. L'objectif principal de cette étude est l'investigation du rôle du frein pour l'atténuation de l'impact maximal du câble porteur. Des nouveaux freins, qui ont été développés à l'HKUST, sont utilisés. La force d'impact dans les barrières flexibles est mesurée par des dynamomètres piézoélectriques qui sont installés sur des ancrages connectés au câble porteur. Le résultat préliminaire indique que les freins installés en une barrière flexible réduisent la force d'impact dans les câbles et augmentent la dissipation d'énergie.

KEYWORDS: debris flows, flexible barrier, impact, brake elements

1 INTRODUCTION

Steep creek flows comprised of poorly sorted mixtures of soil and water, surge downslope in mountainous areas under gravity at high velocities. Such flows often result in fatalities (Froude & Petley 2018) and damage to infrastructure (Jakob et al. 2012). To arrest these flows, intercepting barriers are constructed at the downstream end of a catchment. Over the past decade, flexible barriers for rock fall have been impacted by debris flows and proved to be effective at arresting debris flows (Wendeler et al. 2006, Kwan & Koo 2014). Flexible barriers (Figure 1), initially introduced for intercepting rockfalls, have gained popularity in intercepting various types of geophysical flows such as debris flows (Wendeler et al. 2006), open hillslope failures (Kwan et al. 2014) and snow avalanches (Margreth & Roth 2008). Flexible barriers are generally made up of intercepting net mesh/rings, supporting cables, posts and energy dissipating elements. Flexible barriers undergo large deformation during impact, which prolongs the impact duration and reduces the impact load (Wendeler et al. 2006). Flexible barriers are advantageous for steep terrain because they occupy smaller footprints, are easier to construct and blend in with the natural surroundings compared to reinforced concrete barriers. For effective use of flexible barriers, as structural countermeasures to arrest debris flows, there is clearly a need to understand flow barrier interaction.

Several scientific approaches are used by researchers in physical modelling of debris flow impact on structural countermeasures. Full-scale field tests, scaled flume tests and centrifuge tests are commonly used methods. Currently, only limited studies of full-scale debris flow impact on flexible barriers are reported (Wendeler et al. 2006, Ferrero et al. 2015). Wendeler et al. (2006) reported impact forces induced on instrumented flexible barrier where the cable load time-histories of the horizontal supporting cables are recorded; however, barrier displacement and deformation of energy dissipating elements were not captured. This limits our understanding of debris flow flexible barrier interaction during impact. Furthermore, unique site characteristics in field monitoring hinder interpretation of results which are generally unreproducible (Iverson 2015). To alleviate some of the shortcomings of field idiosyncrasies, Ng et al. (2017) adopted centrifuge modelling with idealized impervious flexible barrier. The idealized model barrier purposefully simplifies the interaction mechanism by ignoring the influence of barrier perviousness and energy dissipating elements. This results in high impact loads. In this study, the influence of energy dissipating elements on attenuating peak impact force of debris

flows on a flexible barrier is systematically investigated in a 2 m wide 28 m-long flume. The use of a 2 m wide flume also addresses the issue of disproportionate scaling of fluid viscous stresses compared to grain frictional stress (Iverson 2015) that are prevalent in small-scale flume modelling.

2 PHYSICAL FLUME MODELLING

A 28 m-long flume (Figure 2) is used to conduct physical experiments to gain new insight on the impact mechanisms of two-phase debris flows against a single flexible barrier. The flume has a uniform rectangular cross-section with a width of 2 m and a depth of 1 m. The side walls are transparent on one side of the flume to enable the impact kinematics to be captured during experiments. A storage container that can hold up to 10 m^3 is inclined at 30° at the top of the flume. The main flume is 15 m in length and has an inclination of 20°. The bottom part of the flume is horizontal and 8 m in length. A double door gate system is used to retain debris material inside the storage container. The doors are secured and released using a mechanical arm, which is controlled by an electric motor.

Figure 1. Flexible barrier (Hong Kong)

Figure 2. Twenty-eight-metre-long debris flow flume at Kadoorie Centre, University of Hong Kong

2.1 *Model setup and instrumentation*

The flexible barrier used in this study has a ring net panel that is 2000 mm wide and 800 mm high. The barrier is installed at an inclined distance of 13.5 m from the gate (Figure 3). Each ring is 100 mm in diameter and made using steel wires that are 2 mm in diameter. The ring net panel is supported by two horizontal cables, which are anchored to the sidewalls of the flume. Tension load cells (TML TCLK50KNB) are used to measure the impact load of each cable. A mesh with 25 mm square openings made of 1 mm diameter stainless steel wire was overlaid onto the ring net to retain the debris material during and after impact. Dual spring elements (Ng et al. 2016; Figures 3 & 4) are installed between ends of cable and anchors at flume side walls using eyebolts to replicate the loading response of an energy dissipating device used in prototype barriers. The dual spring element exhibits a bilinear load-displacement response (Figure 4). Each of the dual spring element comprises two compression springs—one stiff (k_1 = 1380 kN/m; red spring) and the other soft (k_2 = 36 kN/m; green)—in series inside a cylinder. The springs are separated inside the cylinder by a coaxial separator. The flexible spring is preloaded to a specifiable load (P_{pre} = 1.9 kN) by adding a spacer between the spring and separator inside the cylinder. Before the applied load reaches the inflection point (P_{pre}), only the stiff spring resists the load and slope $K_1 = k_1$. After reaching the inflection point, the load is shared by both springs in series and the equivalent stiffness reduces to model the elongation of energy dissipating elements $K_2 = k_1k_2/(k_1 + k_2) = 35$ kN/m. The peak deformation of dual spring elements is preserved by a pneumatic locking system.

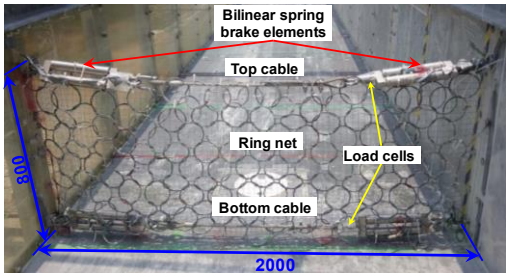

Figure 3. Front elevation of flexible barrier with two brake elements per cable (looking upstream)

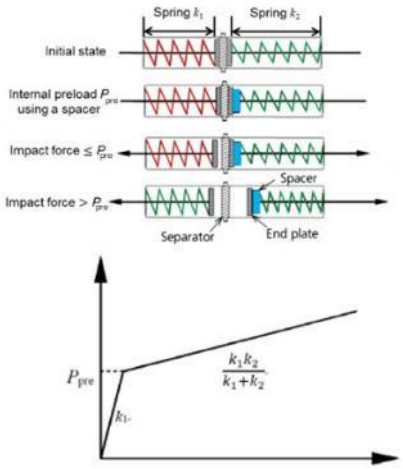

Figure 4. Dual spring element working principle and force-displacement behaviour

In addition to the load cell, the instrumentation used includes laser and ultrasonic displacement sensors (Keyence IL600/IL1000 and Banner TUB30X), mounted above the

channel to measure the flow depth. Furthermore, high-speed cameras (Mikrotron EoSens 4CXP) are used in the 28 m-long flume tests to capture the impact kinematics and an unmanned aerial vehicle (DJI Phantom 3) is used to capture an aerial view of the experiment.

2.2 *Debris material*

The two-phase debris flow material used in this study is representative of the typical debris flow material in East Asia. This mixture generally comprises 35% gravel (20 mm), 62.5% sand (0.6 mm), and 2.5% clay (< 2 μm) (Ng et al. 2019). A solid fraction of 0.6—typical in field debris flows (Iverson 2015)—is adopted for the testing material. The initial density of the mix is approximately 2,000 kg/m^3. Figure 5 shows the particle size distribution (PSD) of the debris material (HKUST SGM) used in this study. The rationale behind choice of debris mixture is to find a reproducible mix that compares well with the particle size distribution of previous debris flows in Hong Kong.

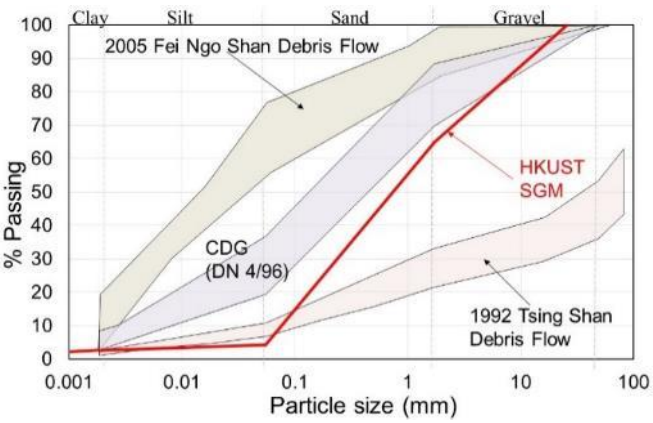

Figure 5. PSD range of previous debris flow events in Hong Kong and the design debris mixture (HKUST SGM)

2.3 *Test programme and procedure*

To investigate the influence of brake elements on the loading response of flexible barrier impacted by debris flows, the brake element configuration is varied for different tests (Table 1). Prior to impact tests, a series of control tests are carried out to characterize the debris flow along the flume. In all the tests, the gates are closed and debris flow mixture is prepared in the storage container. Once the debris mixture is ready, the gates are opened and the debris is allowed to flow downstream simulating a dam break. The instrumentation is started simultaneously as the gate is opened and data is recorded at 2 kHz to capture debris flow interaction with the barrier.

Table 1. Test programme

Test ID[#]	Number of brake elements per cable
DBr0	Nil
DBr1	1 (At one anchor)
DBr2	2 (At both anchors)

[#] Debris volume = 2.5 m^3 in each test

3 INTERPRETATION OF TEST RESULTS

All recorded time-history data are readjusted to an initial time of impact at 0 s in all tests when flow front reaches the barrier.

3.1 *Observed debris flow impact mechanisms*

Figure 6 shows top view of the impact kinematics of debris flow impacting against a single flexible barrier installed orthogonally to the channel bed. Upon impact, the flow jumps along the face of the barrier at t = 0.5 s. Subsequent flow impacts the arrested material while some fines and fluid pass through the pervious flexible barrier. The dual spring elements are activated as the top cable deforms. The run-up follows the curvature of the deformed barrier and rolls back towards the upstream direction at t = 1 s. The original and deformed profiles of the top cable are shown using solid red and dashed white lines, respectively. As more debris deposits at the base of the barrier, the volume of material discharging through the barrier diminishes because the secondary mesh opening is clogged by the coarse gravels in the debris mixture. This process enlarges the dead zone at the base of the barrier. The dual spring elements installed on the top and bottom cables are eventually fully mobilized. The bottom cables are no longer visible in the field of view due to the deformation of the flexible barrier along the flow direction. Overspill is observed at t = 1.5 s. Simultaneously, the rolling back motion of the debris flow front impacts the incoming flow and the dead zone increases in size. At t = 2 s, the roll back diminishes, although overspill still continues. At t = 6.0 s, debris is retained by the flexible barrier with a horizontal free surface up to the fully deformed height of the barrier. The horizontal free surface of the deposit may indicate a fluidized debris material. The fluidization of debris material is further corroborated by the measured basal pore pressure and normal stresses.

Figure 7 shows the time histories of basal total normal stresses, pore pressures and deduced effective stresses in test DBr2. The evolution of basal pore pressures and total normal stresses show that the debris deposit is nearly fluidized with an average pore pressure ratio $(\mathrm{u_w}/\sigma)$ of around 0.99 at the end of the impact process at t > 9 seconds. Furthermore, the measured basal shear stress ($\tau_{\mathrm{b,meas}}$ = 0.8 kPa) at the end of the impact (t > 5 s) is used in back calculating a bed friction angle (δ_{b}) of 4 ° $\left[\delta_{\mathrm{b}} = \tan^{-1}(\rho g h \cos\theta/\tau_{\mathrm{b,meas}})\right]$. The measured pore water pressure is almost double the hydrostatic value, deduced from measured flow depth, showing generated excess pore pressure at the end of impact (t > 5 s). In light of these facts, the total lateral earth pressure coefficient can be assumed to be unity in estimating load of static deposit on the barrier. The excess pore water pressure reduces the effective stress of the soil such that inter-granular friction is reduced and the debris material is essentially fluidized. Consequently, with loss of frictional resistance, the lateral earth pressure coefficient tends to unity.

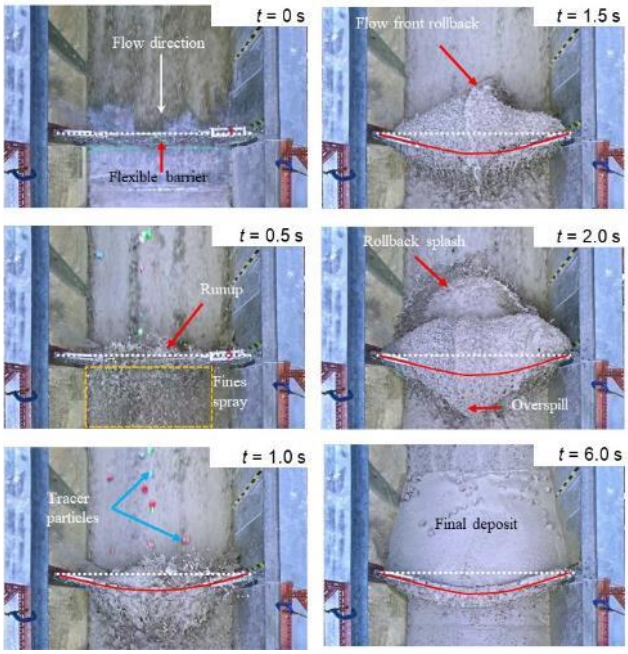

Figure 6. Observed interaction kinematics of debris flows with flexible barrier in tests DBr2.

The observed kinematics of debris flow impacting against the model flexible barrier exhibits characteristics of both run-up and pileup mechanism reported by Choi et al. (2015). Initially, the observed impact process in this study is reminiscent of the run-up mechanism. Near the end of impact, the observed impact mechanism resembles the pileup mechanism. The transition from run-up to pileup occurs when the roll back impacts the incoming flow body and starts to propagate upstream. In tests with different brake element configurations (tests DBr0 & DBr1), the impact mechanism is similar to that reported for DBr2 albeit the run-up height is lower. The debris flow progressively accumulates behind the barrier as a reflected wave is formed and propagates upstream.

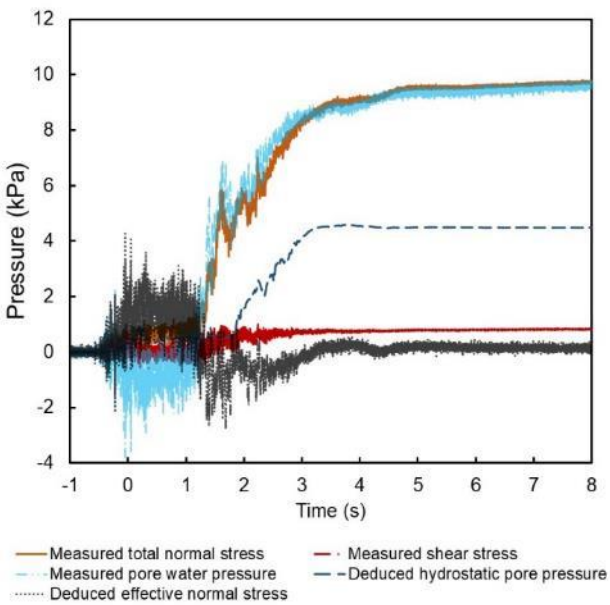

Figure 7. Time-history of basal stresses and pore pressure readings in test DBr2

3.2 *Measured cable loads and deflections*

Figure 8a shows the time-history of measured cable tension in test DBr2. The bottom cable experiences frontal impact as the flow front reaches the barrier. As the fine particles and fluid in the debris flow front partially pass through the barrier mesh, small perturbations are recorded by the load cells. At t = 0.5 s, both the bottom and top load cells register a short spike which corresponds to the flow front run-up along the barrier as shown in Figure 6 (t = 0.5 s). The tension force in both the bottom and top cables increase simultaneously until t = 1 s. The slight flattening of the loading curves is because the activation of the energy dissipating brake elements as P_{pre} (Figure 4) was reached. As the impact process continues, the loading on the top and the bottom cables diverge. The bottom cable experiences continued dynamic impact from incoming flow in addition to the static load due to flow run-up. As such, the tension in bottom cable increases rapidly, compared to the top cable. The brake elements in the two cables reach their design deformation capacity at t = 1.2 s and t = 1.4 s respectively. This is evident in the cable load time-history, resulting in a change of loading rate. The debris barrier interaction continues, and the top cable experiences a peak dynamic force of 4.1 kN as the flow attains maximum run-up height. The maximum run-up height occurs at t = 1.8 s and the flow front at this time has rolled back upstream splashing onto the incoming flow. As the run-up falls back towards the channel, the barrier rebounds and the tension force in the cables relaxes. This load relaxation is more pronounced in the top cable, where the static load has a minimal effect compared to that in the bottom cable. As the flow run-up falls back on the incoming flow, a stress wave is formed that propagates upstream from the barrier. This stress wave intercepts the incoming flow and dissipates the flow kinetic energy such that the debris material piles up enlarging the deposit volume. Debris accumulates at the base of the barrier and the bottom cable tension increases to a peak value of 7.2 kN at t = 8 s with the formation of a static deposit at the end of impact.

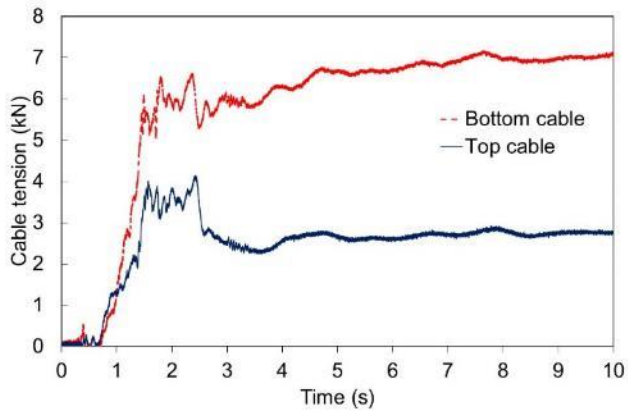

(a)

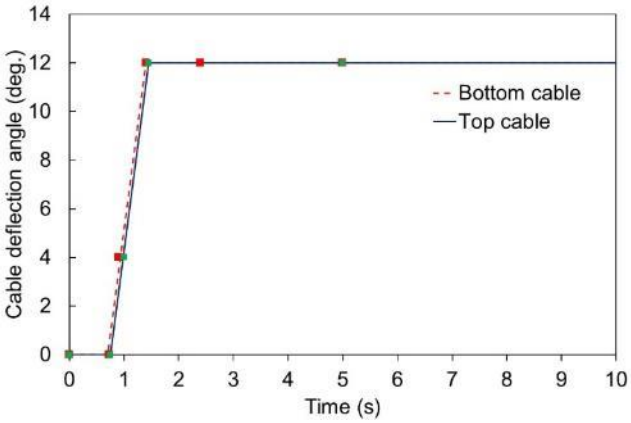

(b)

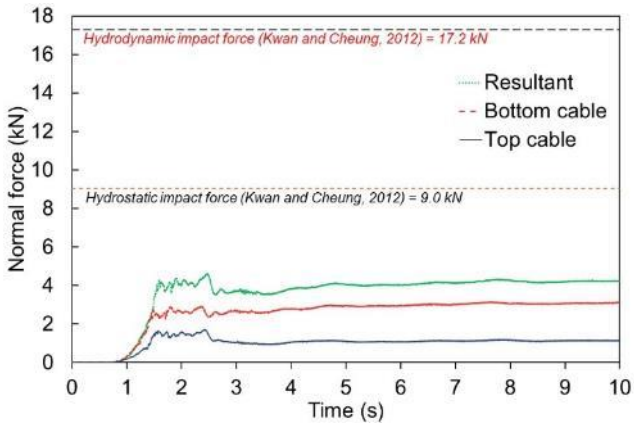

(c)

Figure 8. Time-histories of (a) cable tension (b) deduced cable deflection angle at support (c) deduced normal force in test DBr2.

Figure 8b shows the time-history of cable deflection angles deduced from top view video recording of barrier deformation. The deflection angles are deduced by tracking the deformed configuration of the cable over the span of the impact process. The tracking of the deformation angle for top cable is straight forward as the top cable is clearly visible for the entire duration of the test. The final cable deflection angle of 12 degrees is the maximum deflection angle deduced from video analysis and corroborated by measurement after the test. In the case of bottom cable, the deflection angle measured after the test is 12 degrees. Since the deformation of the barrier mesh obstructs the view of bottom cable in the video, we assume the bottom cable deflection time history to be identical to that of the top cable. The deduced final cable deflection angles are verified with measured values. Both the measured and deduced values are found to be identical. The cables deformed as a circular arc by the end of the test (see Figure 6; t = 6.0 s). This circular deformation of the cable implies that the pressure acting on the cable is perpendicular to its profile (Song 2016). The deduced cable deflection angles are used in calculating impact load normal to the barrier.

Figure 8c shows the time-history of deduced barrier normal forces for top and bottom cables and the resultant normal force. Song (2016) calculated the normal force acting on the barrier by assuming the barrier deformed in the shape of a circular arc. Based on the measured cable tension and deflection angle, the normal forces acting on the barrier was deduced. The deduced peak resultant normal force is 4.6 kN, while the hydrodynamic impact force estimated using existing design guideline in Hong Kong (Kwan & Cheung 2012) is 17.2 kN. The estimated design hydrodynamic impact force is more than 3 times higher than that measured in this study. Similarly, the design hydrostatic force is 2 times larger than the measured one. This difference could be attributed to the load model assumptions where internal shearing within the debris material in the hydrodynamic model is ignored and the allowance for boulder impact (see also discussion in Section 3.3). In the case of design hydrostatic forces, the shearing resistance of debris material is ignored by assuming lateral earth pressure coefficient of unity. Also, the design value takes into account for the impact loadings of sizeable boulders. It can be observed that the dynamic impact at peak run-up (t = 2.5 s) results in the maximum normal force on the barrier. This shows that the peak impact force does not necessarily coincide with the frontal impact of debris flows but also includes static load due to run up. In other test cases, the impact process evolves qualitatively in the same manner as described above. The impact mechanisms mainly differ in the peak run-up height and deposition processes. The interaction mechanisms—run up versus pile up—must be considered in estimating the peak impact force, which is missing from existing load models (Kwan & Cheung 2012, Wendeler et al. 2019). The Hong Kong design guideline TGN-44 (GEO 2015) provides an updated recommendation in the surge-by-surge calculation method for debris flow impact. TGN-44 recommends the use of cumulative debris flow hydrograph and velocity hydrograph to accommodate the wedge shaped deposit during impact process and reduced flow velocity for each surge in estimating the impact force. This allows the designer to identify the peak load when the barrier is progressively filled in a pile-up process. Run up of debris flow from subsequent surges are not considered in the design.

3.3 *Influence of brake elements on peak impact load*

Figure 9 shows the deflection of the load bearing cables and the barrier mesh resulting from different normal impact forces. The measured peak deflection of the cables and the barrier mesh are normalized by the barrier span (L) while the peak normal impact force is normalized by the hydrodynamic impact force (Kwan & Cheung 2012). The hydrodynamic impact force is defined as:

$$F_{\text{dyn}} = \alpha \rho v^2 h w \tag{1}$$

where α is the hydrodynamic pressure coefficient, $\rho = 2000\ \text{kg/m}^3$ is the bulk density of debris flow, $v = 6\ \text{m/s}$ is the velocity of debris flow front impacting the barrier, $h = 0.06\ \text{m}$ is the average flow depth of the debris flow and $w = 2.0\ \text{m}$ is the flume width. Kwan & Cheung (2012) proposes a hydrodynamic impact pressure coefficient of 2 for the design of flexible barriers subjected to debris flow impact which also takes into account the effects of sizeable boulder impact. This is shown on as the as a vertical reference line in the plot. However, results of current study show that the measured normalized peak impact force (used as a measure of the hydrodynamic pressure coefficient) is 1.1 for flexible barrier without any brake elements. For tests with brakes, this pressure coefficient is much lower around 0.6. This discrepancy of more than 80% in the normalized peak impact force indicates there is room for optimizing the alpha value for soil debris without sizeable boulders.

The square, circular and triangular markers represent data points for tests DBr2, DBr1 and DBr0 respectively. The size of the markers corresponds to the magnitude of the normalized deflection and impact force. The largest markers (black) represent the barrier mesh, the intermediate markers (red) represent the bottom cable and the smallest markers (green) represent the top cable. In all the tests, it is observed that the barrier mesh has the largest deflection followed by the bottom and top cable respectively. Furthermore, test DBr2 with two energy dissipating elements has the largest normalized peak barrier and cable deflections compared to test DBr1 and DBr0. The peak deflection of the bottom cable in test DBr2 is 30% larger than that measured in test DBr1 and 80% larger than in test DBr0. The influence of larger barrier deflections is reflected in the decreasing trend of the normalized peak impact force in test DBr2 compared to test DBr1 and DBr0. The normalized peak impact force in the case of test DBr0, DBr1 and DBr2 are 1.10, 0.64 and 0.57 respectively. Use of two brake elements per cable reduces the peak normal impact force by 50% compared to the test with no brake elements in the cables. The increased barrier and cable deflection during impact reduces the relative velocity between the incoming flow and the barrier. The deflection of the barrier increases the impact duration and allows increased internal shearing of the flow by

promoting frictional dissipation (Ng et al. 2020). The relative velocity between the flow and the deflected barrier leads to a decrease in momentum transfer during impact. The outflow of fine materials through the mesh opening and the curvature of the deflecting barrier further reduces momentum transfer from the flow. These combined processes result in lower impact force on a flexible barrier that undergoes larger deformation.

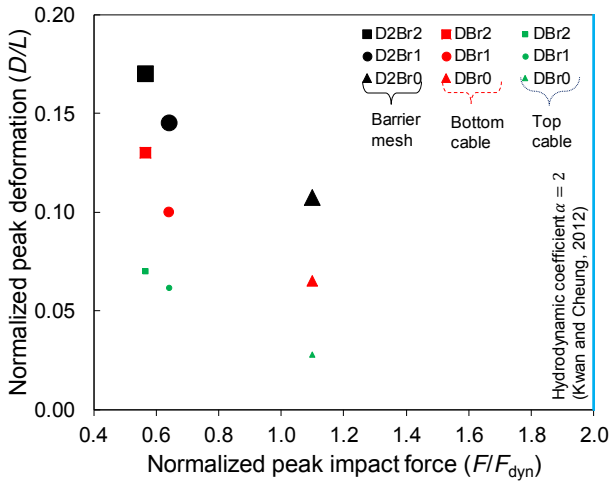

Figure 9. Effects of brake elements on normalized peak deflection and peak impact force

4 CONCLUSIONS

A series of physical experiments modelling the impact of channelized debris flow on a side anchored flexible barrier was conducted in a state-of-the-art 28 m-long flume. Novel energy dissipating elements developed in-house are used to vary the stiffness of the load bearing cables. A large deflection of the load bearing cables and mesh (*D/L*> 5%), due to the mobilization of brake elements, results in the attenuation of the peak impact force induced on the barrier by up to 50 % compared to flexible barriers without brake elements. Compared to flexible barrier without brake elements, the mobilization of brake elements results in an attenuated barrier loading response and prolongs internal shearing of the granular material in the debris material.

5 ACKNOWLEDGEMENTS

The work described in this paper was supported by two grants from the Research Grant Council of the Government of Hong Kong Special Administrative Region, China (T22-603/15-N and AoE/E-603/18). S. Poudyal gratefully acknowledges the support of Hong Kong PhD Fellowship Scheme (HKPFS) provided by the RGC of HKSAR, China. This paper is published with the permission of the Head of the Geotechnical Engineering Office and the Director of Civil Engineering and Development, the Government of the Hong Kong Special Administrative Region, China.

6 REFERENCES

Choi C.E., Au-Yeung, S.C.H., Ng, C.W.W., and Song, D. 2015. Flume investigation of landslide granular debris and water runup mechanisms. *Géotechnique Letters 5*(1), 28-32.

Ferrero A.M., Segalini A. and Umili M. 2015. Experimental tests for the application of an analytical model for flexible debris flow barrier design. *Engineering geology*, 185, 33-42.

Froude M.J. and Petley D.N. 2018. Global fatal landslide occurrence from 2004 to 2016. *Nat. Hazards Earth Syst. Sci.,* 18:2161–2181

GEO (2015) Assessment of Landslide Debris Impact Velocity for Design of Debris-resisting Barriers (GEO TGN 44). *Geotechnical Engineering Office, Civil Engineering and Development Department, The HKSAR Government.*

Iverson R.M. 2015. Scaling and design of landslide and debris-flow experiments. *Geomorphology* 244:9–20

Jakob M., Stein D and Ulmi M. 2012. Vulnerability of buildings to debris flow impact. *Nat Hazards* 60:241–261

Kwan J.S.H., and Koo R.C.H. 2015. Enhanced Technical Guidelines for Design of Debris-resisting Barriers. *GEO Report No. 333. Geotechnical Engineering Office, Civil Engineering and Development Department, The HKSAR Government*.

Kwan J.S.H. and Cheung R.W.M. 2012. Suggestion on design approaches for flexible debris-resisting barriers. *Discussion Note DN1/2012. Geotechnical Engineering Office, Civil Engineering and Development Department, The HKSAR Government*.

Margreth S. and Roth A. 2008. Interaction of flexible rockfall barriers with avalanches and snow pressure. *Cold regions science and technology*, 51(2-3), 168-177.

Ng C.W.W., Choi C.E., Majeed U., Poudyal S., and De Silva W.A.R.K. 2019. Fundamental framework to design multiple rigid barriers for resisting debris flows. *In: Proc. 16th Asian Reg. Conf. on Soil Mech and Geo. Eng 14th to 18th October 2019. Taipei, Taiwan, China*

Ng C.W.W., Wang C., Choi C.E., De Silva W.A.R.K. and Poudyal S. 2020. Effects of barrier deformability on load reduction and energy dissipation of granular flow impact. *Comput. Geotech,* 121, 103445.

Ng C.W.W., Song D., Choi C.E., Koo R.C.H. and Kwan J. S. H. 2016. A novel flexible barrier for landslide impact in centrifuge. *Géotechnique Letters*, 6(3), 221-225.

Ng C.W.W., Song D., Choi C.E., Liu L.H.D., Kwan J.S.H., Koo R.C.H., and Pun W. K. 2017. Impact mechanisms of granular and viscous flows on rigid and flexible barriers. *Canadian Geotechnical Journal*, 54(2), 188-206.

Pun W.K. and Ho K.K.S. 1996. Analysis of triaxial tests on granitic saprolite performed at Public Works Central Laboratory (Discussion Note DN 4/96*). Geotechnical Engineering Office, Hong Kong*, 72 p.

Song D. 2016. Mechanisms of debris flow impact on rigid and flexible barriers *(Doctoral dissertation), The Hong Kong University of Science and Technology*.

Wendeler C., McArdell B.W., Rickenmann D., Volkwein A., Roth A. and Denk M. 2006. Field testing and numerical modeling of flexible debris flow barriers. *In Proc of the 6th Intl. Conf. on Phys. Mod. in Geo., Hong Kong*, 1573–1578

Wendeler, C., Volkwein, A., McArdell, B.W. and Bartelt, P. 2019. Load model for designing flexible steel barriers for debris flow mitigation. *Canadian geotechnical journal,* 56(6), 893-910.